ADVANCED MATERIALS TECHNOLOGIES

Supporting Information

for *Adv. Mater. Technol.,* DOI: 10.1002/admt.202100700

Spatially Controlled 3D Printing of Dual-Curing Urethane Elastomers

*Brian M. Howell, Caitlyn C. Cook, Michael D. Grapes, Karen Dubbin, Emily L. Robertson, John D. Sain, Kyle T. Sullivan, Eric B. Duoss, and Eric V. Bukovsky**

WILEY-VCH

Supporting Information

Spatially Controlled 3D Printing of Dual-Curing Urethane Elastomers

*Brian M. Howell[1], Caitlyn C. Cook[1], Michael D. Grapes, Karen Dubbin, Emily L. Robertson, John D. Sain, Kyle T. Sullivan, Eric B. Duoss, Eric V. Bukovsky**

This work was performed under the auspices of the U.S. Department of Energy by Lawrence Livermore National Laboratory under Contract DE-AC52-07NA27344. LLNL-JRNL-821071

Supporting Results and Discussion

Cure Depth Analysis: UV rheology was performed on UGAP-NaCl inks following the same procedure in the main text. Gap thickness (0.140–0.840 mm) was varied to determine the effect of solids light scattering on cure depth while representing a decreasing diameter DIW filament exposed to UV light (Figure S6). The gelation point decreases with decreasing gap thickness alluding to a lack of complete 840μm deep light penetration during the ~10 second light exposure during printing. However, when performing a dark polymerization experiment on a 140μm thick sample, further 8 seconds of curing was observed following the removal of the light at 10 seconds. This is representative of the chain-growth kinetics in acrylate radical photopolymerization kinetics and gives reason to believe that acrylate conversion proceeded past the penetration depth of the light in an 840μm diameter filament.

Extent of Dual Curing: Acrylate and urethane degree of cure were measured using FTIR spectroscopy (FTIR, Platinum ATR, Bruker, Figure S8) showing that the acrylate peak (810 cm^{-1}) disappears almost completely with UV-exposure while the isocyanate peak at (2272 cm^{-1}) remains unchanged. As expected, the sample exposed to UV radiation and subsequent heat curing at 80 °C resulted in both peaks disappearing.

X-ray Computed Tomography: The data collection was performed using a North Star Imaging (NSI) X25 computed tomography (CT) system. The Hamamatsu L12161-07 x-ray source was operated with a high voltage of 70 kV, a current of 140 μA, and the "small" focal spot selected. No beam filter was used. The Varian panel detector was operated in its "01_1x10.pFVG1" mode, at a 1.5 frame-per-second integration rate, with a 1920-pixel x 1536-pixel region of interest, with its native pixel size of 127 μm, and with 16-bit data values. The system geometry consisted of source-to-object and source-to-detector distances of 80 and 640 mm, respectively. The corresponding magnification factor was 8X and effective pixel size at the

sample was 15.88 µm. The estimated source focal spot blur was 0.54 pixel. The sample fixturing consisted of a custom additively-manufactured plastic component – a base ("C-2"), a Teflon cylindrical post, and a capped plastic vial. A helical CT scan was executed and consisted of 11,520 projections over a height of 87 mm with an effective angular sampling rate of 1/4 degree. Frame averaging of 2 was used for the projections. The data sets were reconstructed using the NSI-provided commercial software package. No beam-hardening correction was used, the range of gray levels in the reconstructed data was selected to provide good image contrast for the sample material, and the reconstructed data was exported in "stacks" of 8-bit vertical slices and both 8- and 16-bit horizontal slices.

Dynamic Mechanical Analysis: DMTA measurements were performed on a TA Instruments Ares G2 rheometer in tensile torsion mode at a frequency of 1Hz and a strain of 0.1%. Heating was applied at a 5˚C min^{-1} ramp rate when ramping from -110˚C to the end temperature of 50˚C in order to determine the glass transition temperature (T_g) of the elastomeric samples with and without the minor acrylate component crosslinking. Sample dimensions and procedure for DMTA followed ASTM D7028.

Tensile Testing: Tensile specimens (ASTM D-638 Type IV) were tested on Instron 5943 equipped with a 1-kN load cell. Samples were tested under uniaxial tensile loading crosshead speed of 1 mm min^{-1}.

Cell growth and fluorescence microscopy: Extracellular matrix (ECM) protein and plasma treatment was performed by heat treating the porous UGAP material with heat at 200 °C for 2 hours, followed by 150 W for 3 minutes of O_2 plasma in Nordson Asher chamber. Once completed, samples were immediately submerged in sterile ECM protein solution (0.1wt% Fibronectin from human plasma, Sigma, F0895) and incubated at 4 °C overnight. Samples were dried and seeded with normal human lung fibroblasts in fibroblast growth media-2 (FGM-2, Lonza CC-3132). Seeded samples were cultured in a humidified incubator maintained at 37°C with 5% CO_2 for one week.

Supporting Tables and Figures

Table S1: Explicit formulation for urethane grafted acrylate polymer (UGAP) resin in fractional wt%.

8025D	8025E	HDDA	EGPEA	Irgacure 819	EEBCRYL 4396
40.84%	**4.08%**	**1.68%**	**15%**	**3.33%**	**35.07%**

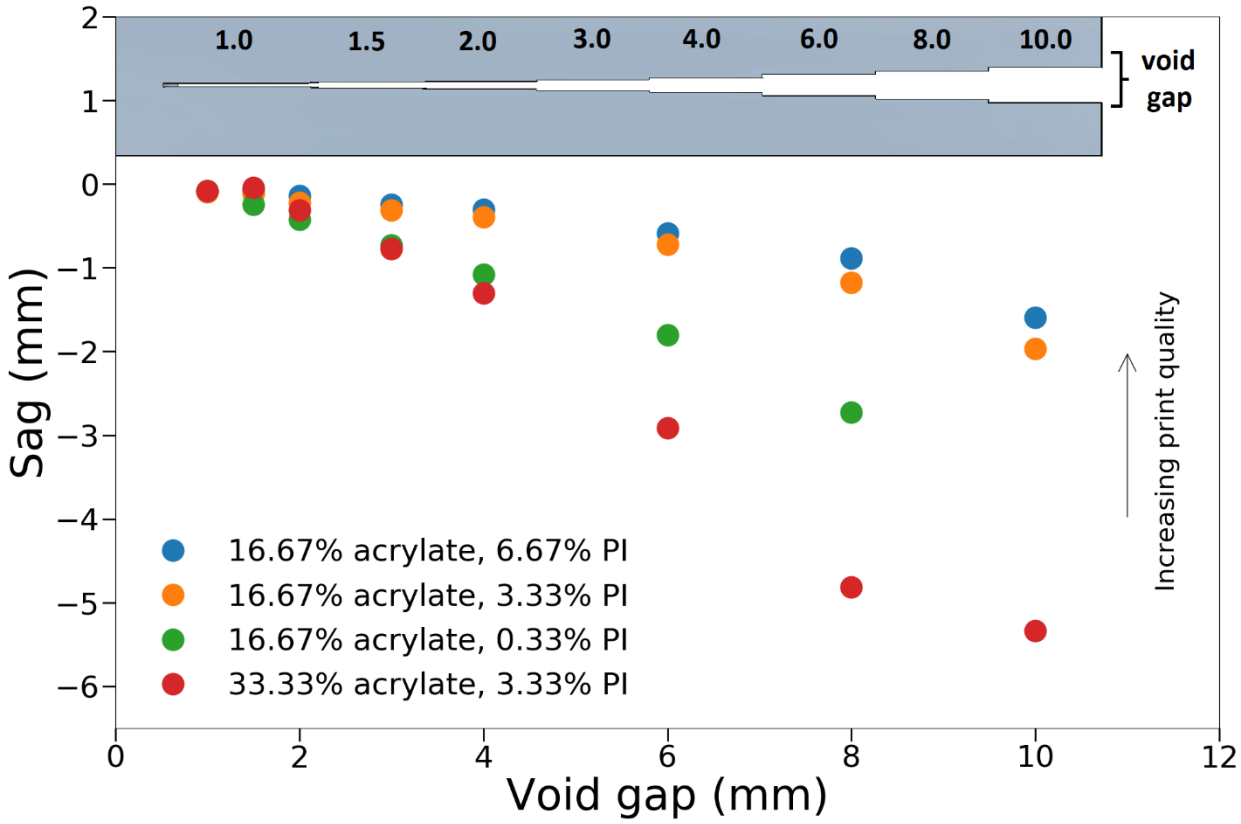

Figure S1: Spanning tests of 70wt% UGAP-NaCl with variable amounts of acrylate and photoinitiator (PI) overlaying a model of a spanning block (varied wt% with respect to resin without solids). Diagram at the top of the graph represents the spanning test block with increasing void gaps in mm.

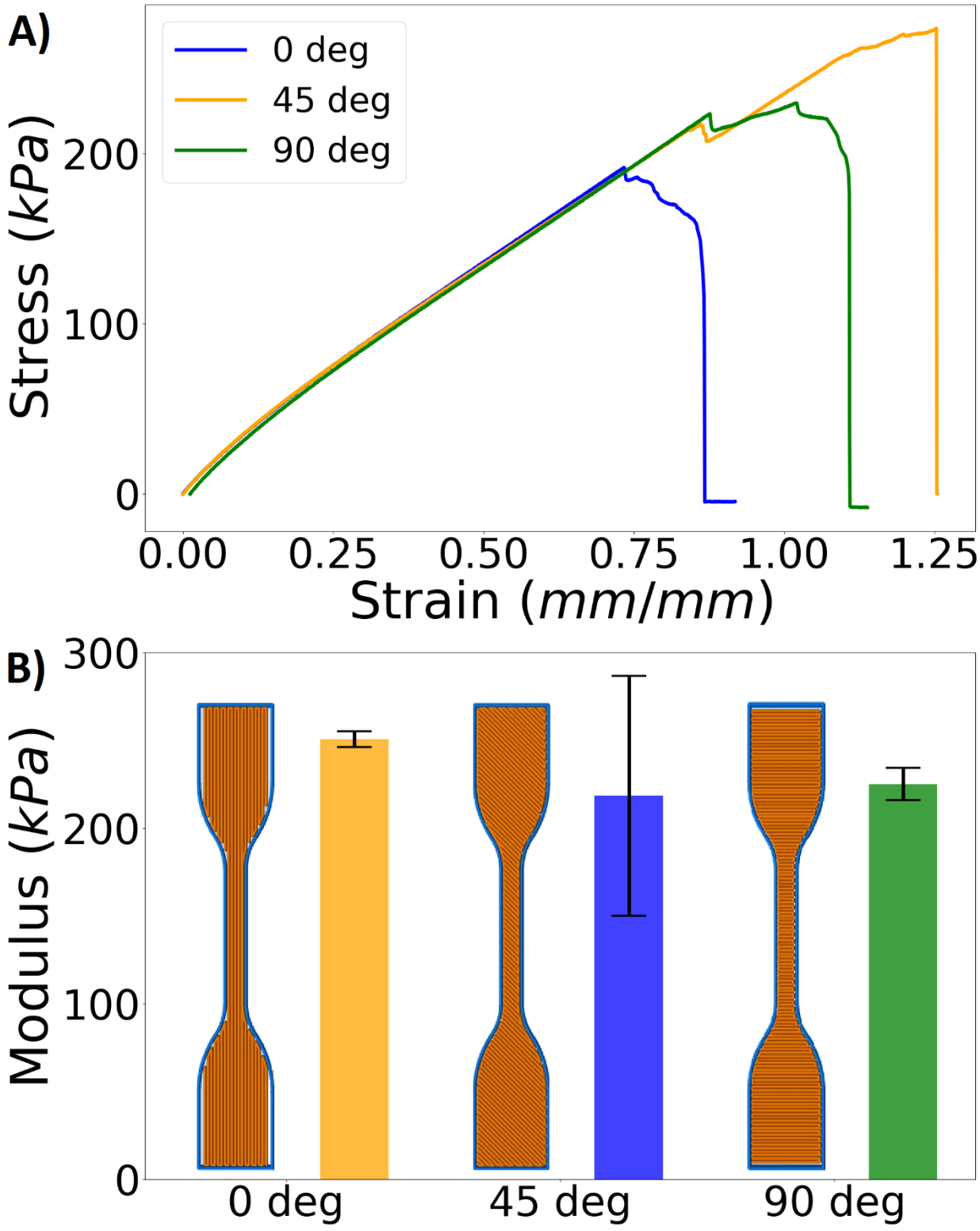

Figure S2: Tensile test of Type IV dog bones printed with different toolpaths. A & B) The stress-strain curves and corresponding tensile moduli of specimens printed with 0-, 45- and 90-degree orientations. Tensile samples failed slowly in multiple areas, as indicated by the step-wise failure in (A).

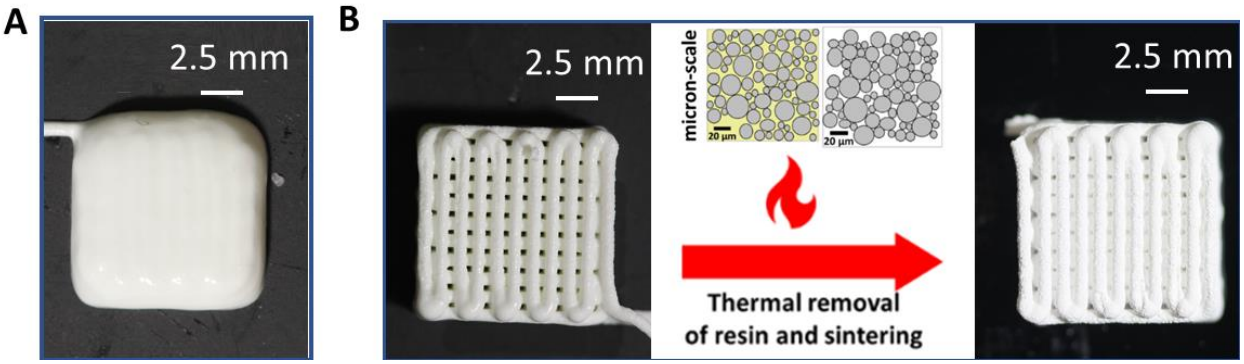

Figure S3: Printing Al_2O_3 filled UGAP. A) Printing a lattice with UGAP- Al_2O_3 without UV light. B) Printing a lattice with UGAP- Al_2O_3 with UV light and subsequently thermally removing UGAP resin and sintering Al_2O_3 particles.

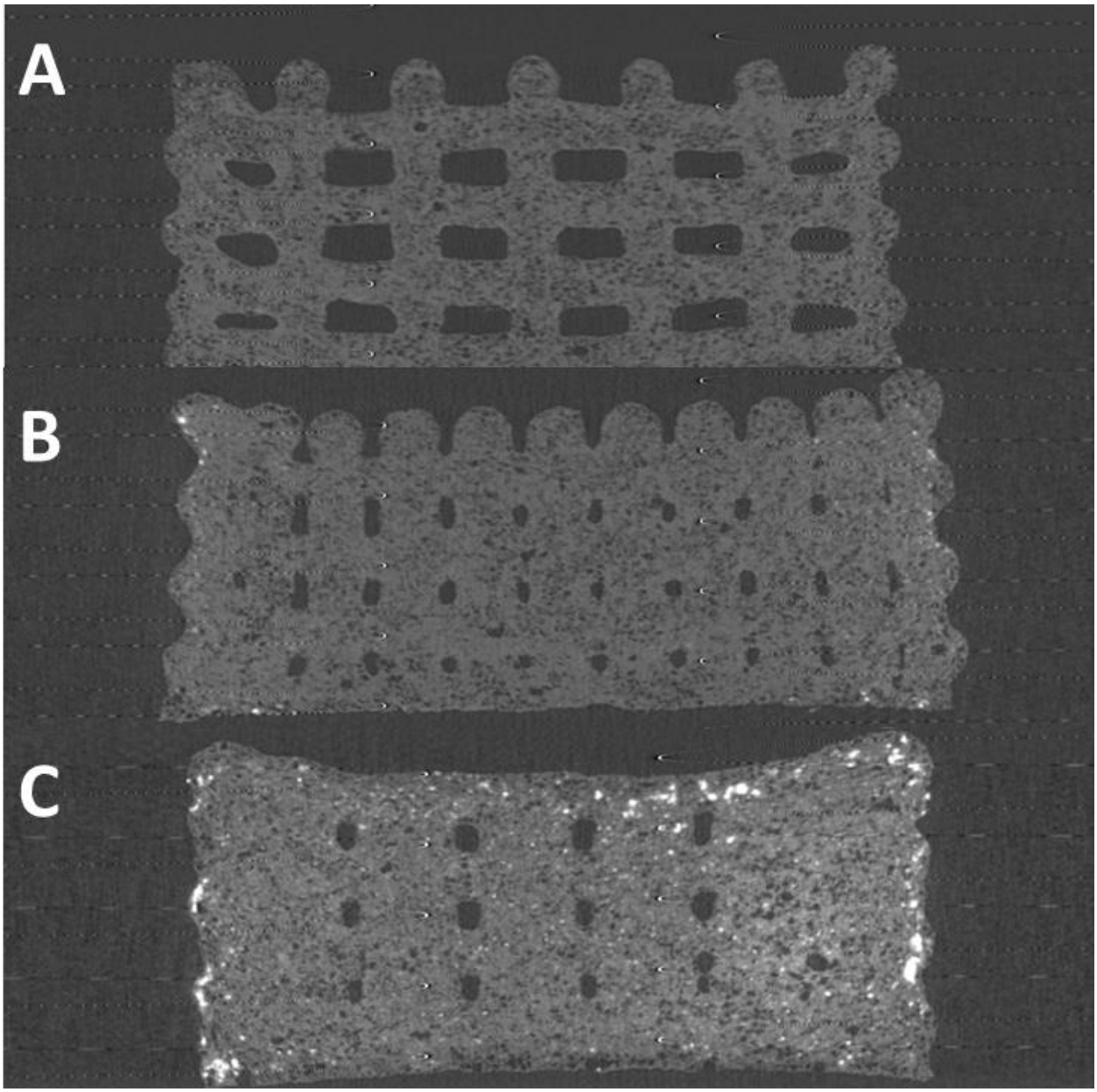

Figure S4: X-ray CT of printed samples leached of salt particles with lattice densities of A) 40%, B) 60% and C) 80% indicating full removal of salt particles and the resulting hierarchical porosity.

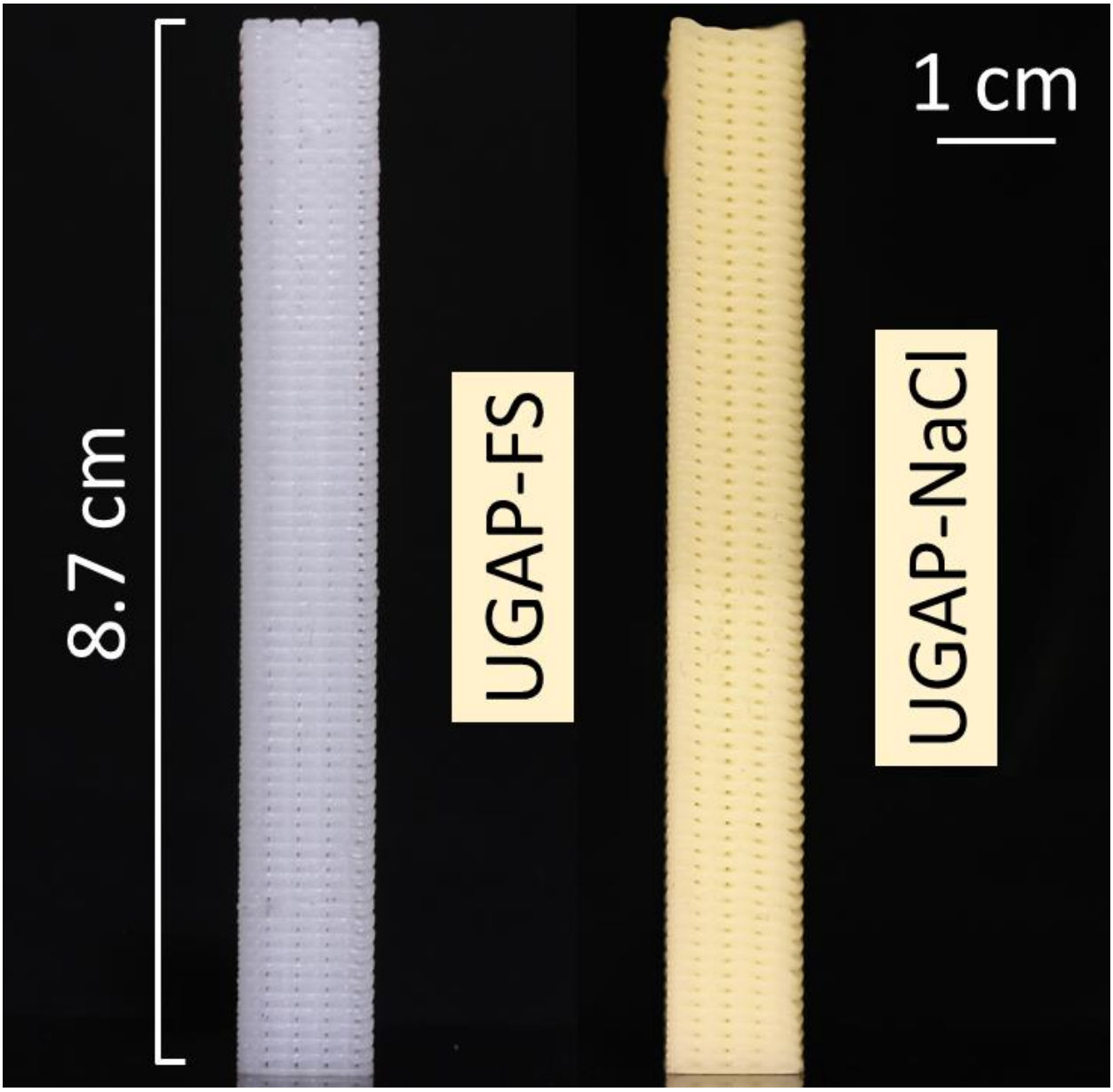

Figure S5: Direct visual comparison of 1 cm x 1 cm towers printed to a height of 8.7 cm with 15wt% UGAP-FS and UGAP-NaCl.

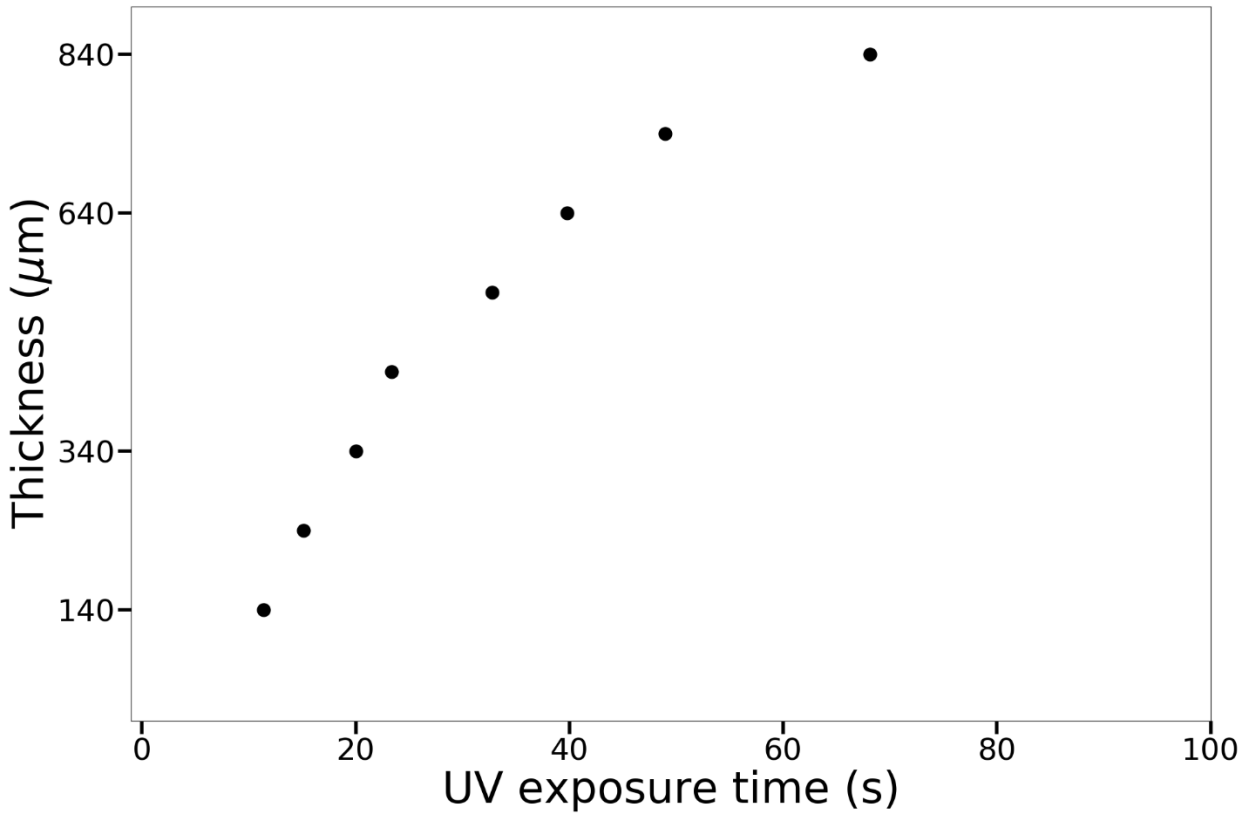

Figure S6: Time to gelation at a consistent 0.6mWcm^{-2} for varying parallel plate gap thicknesses where gelation is defined when $G' = G''$.

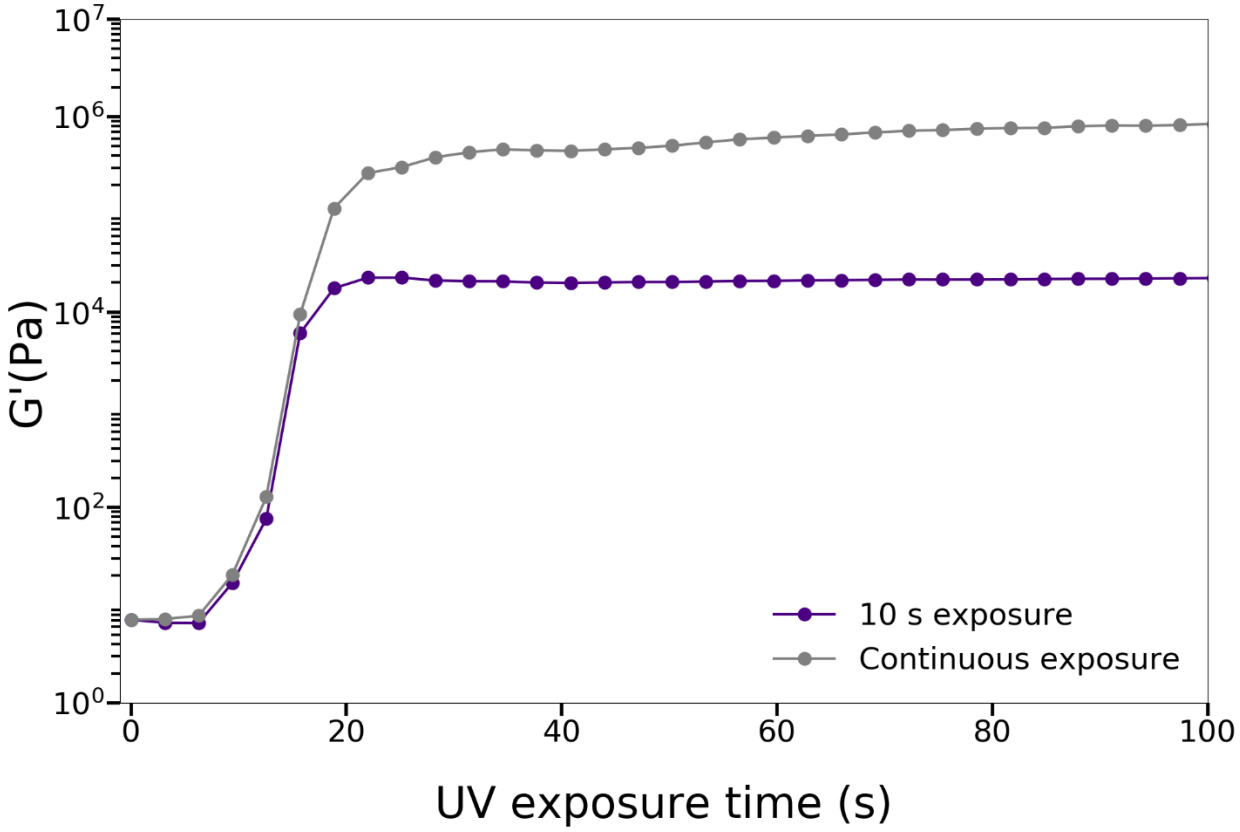

Figure S7: Gelation with time for a 140µm sample continuously exposed to 0.6mWcm^{-2} UV light vs samples exposed to only 10 seconds of UV light, indicating continued dark curing.

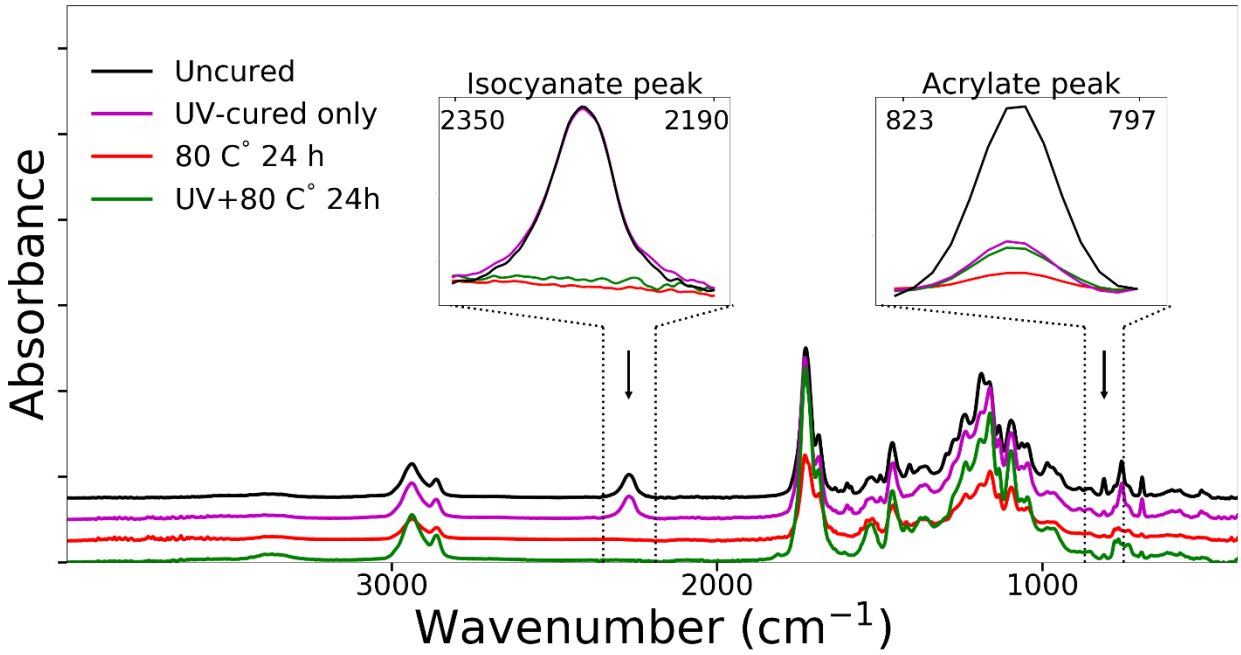

Figure S8: Fourier Transform (FT) IR of UGAP resin samples (i) uncured, (ii) UV-only cured, (iii) heat-only cured at 80 °C, and (iv) UV, then heat cure.

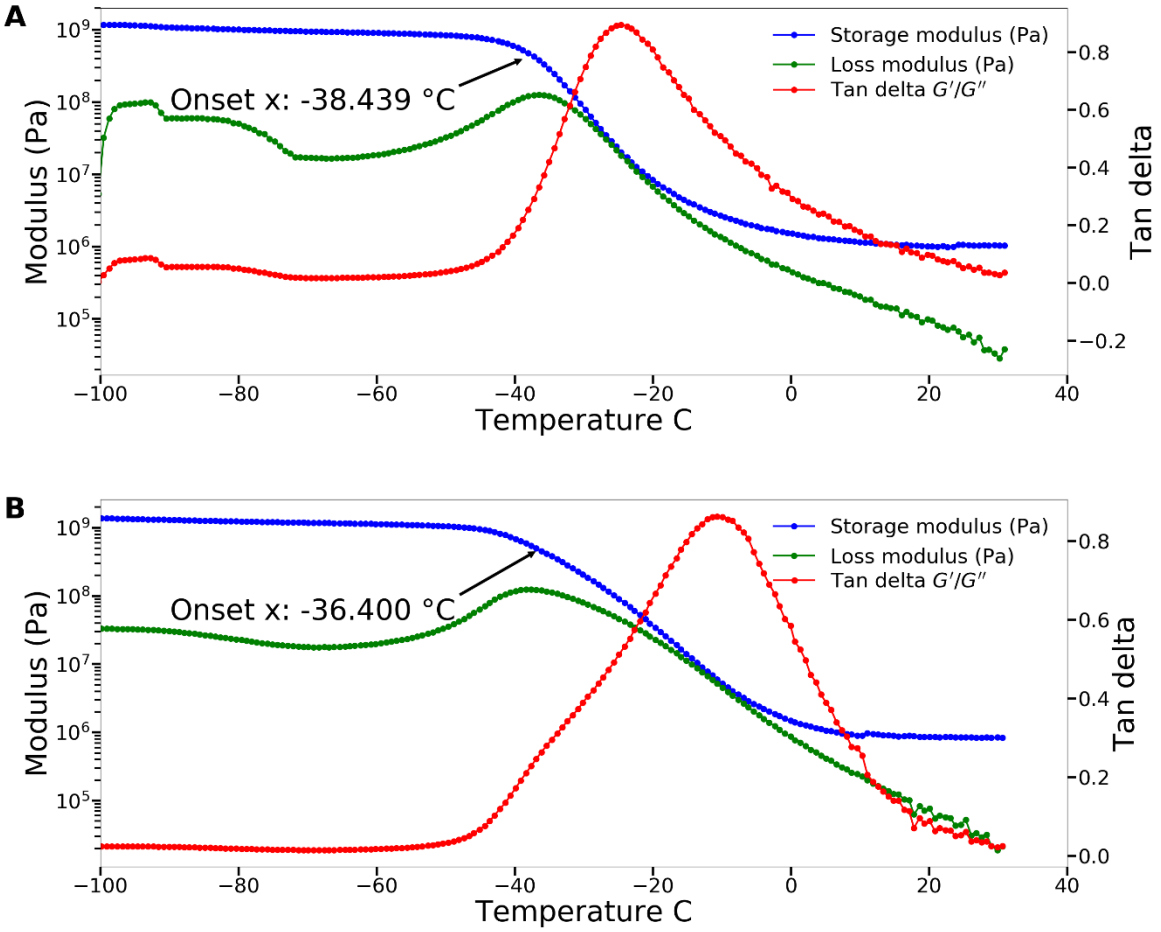

Figure S9: A) Just the urethane components without the minor acrylate cross-linker is cured with heat to confirm a single elastomeric glass transition temperature. B) Adding in the minor acrylate component and dual curing with UV and heat maintains a single glass transition temperature while maintaining a dominant elastomeric property.

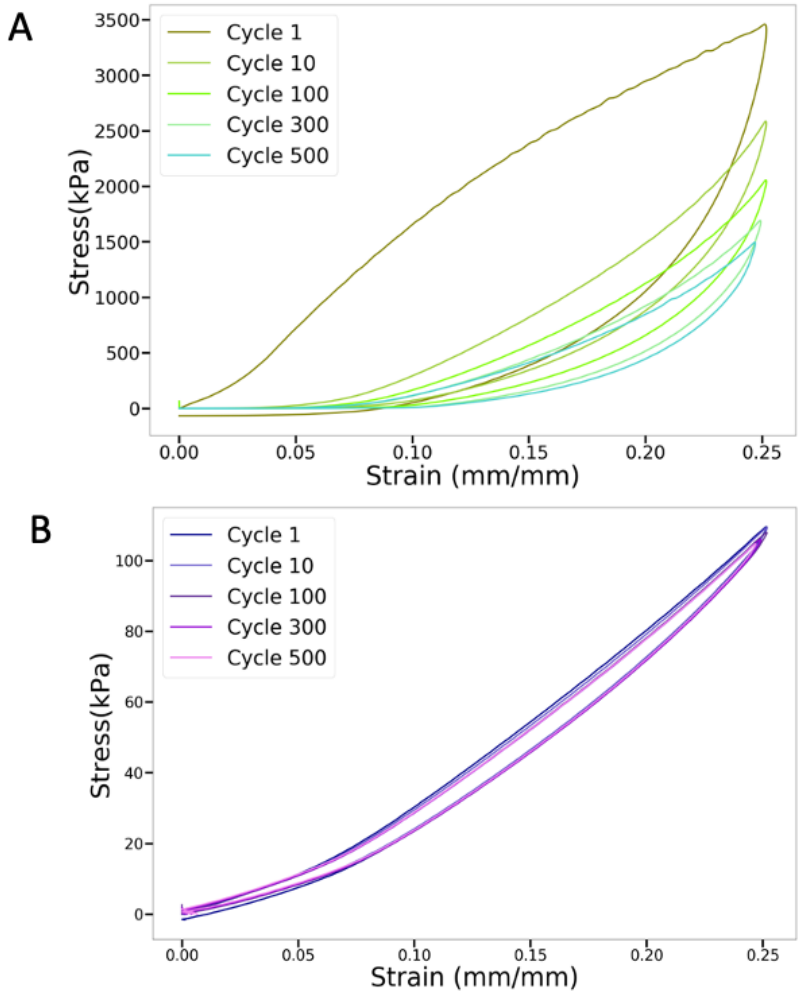

Figure S10: Iterative compression cycles of 1 cm x 1 cm x 0.5 cm 60% lattice density structures printed with A) 70wt% UGAP-NaCl and B) leached NaCl pores.

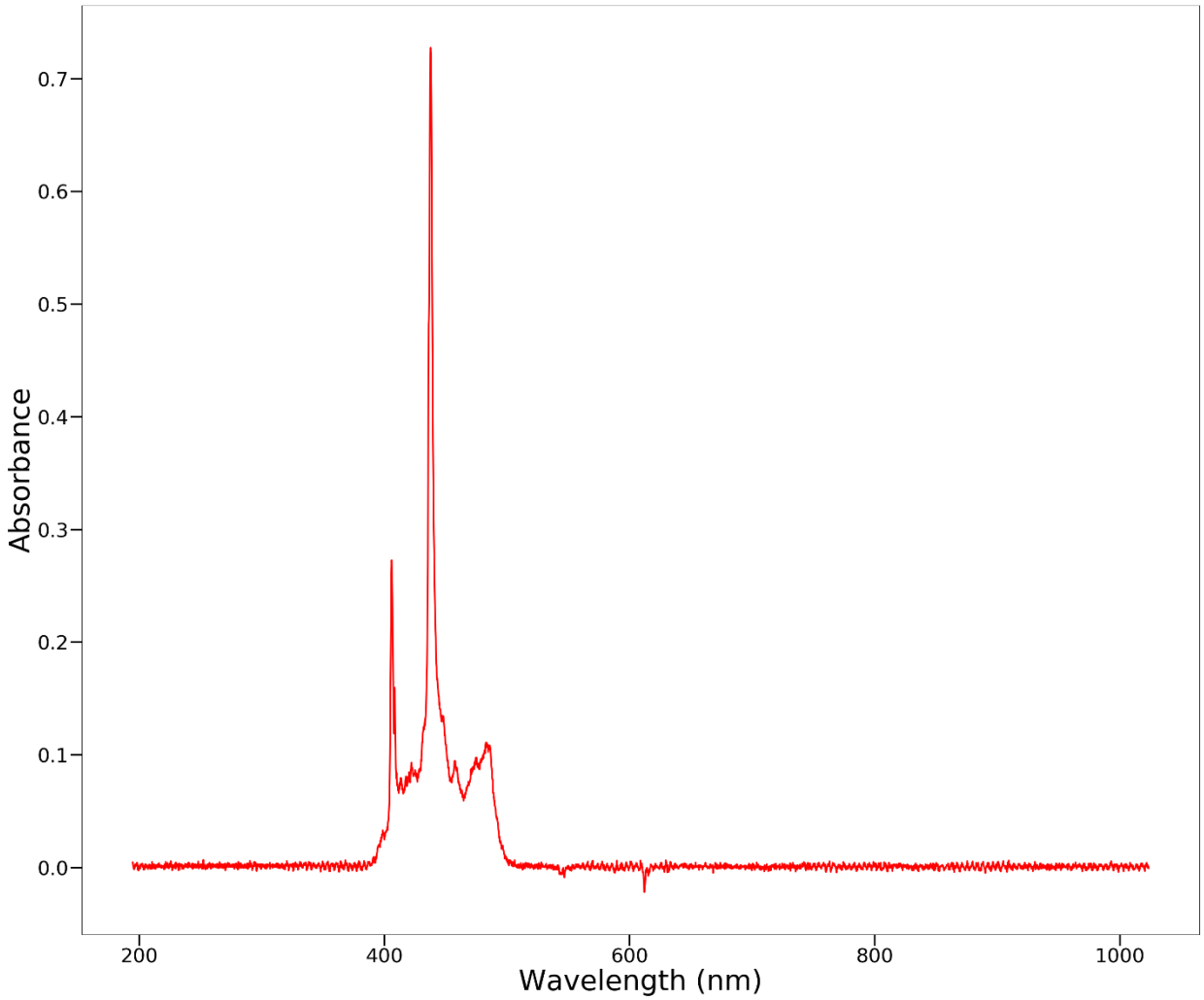

Figure S11: UV spectrum of Omnicure S2000 with 400-500 nm filter.

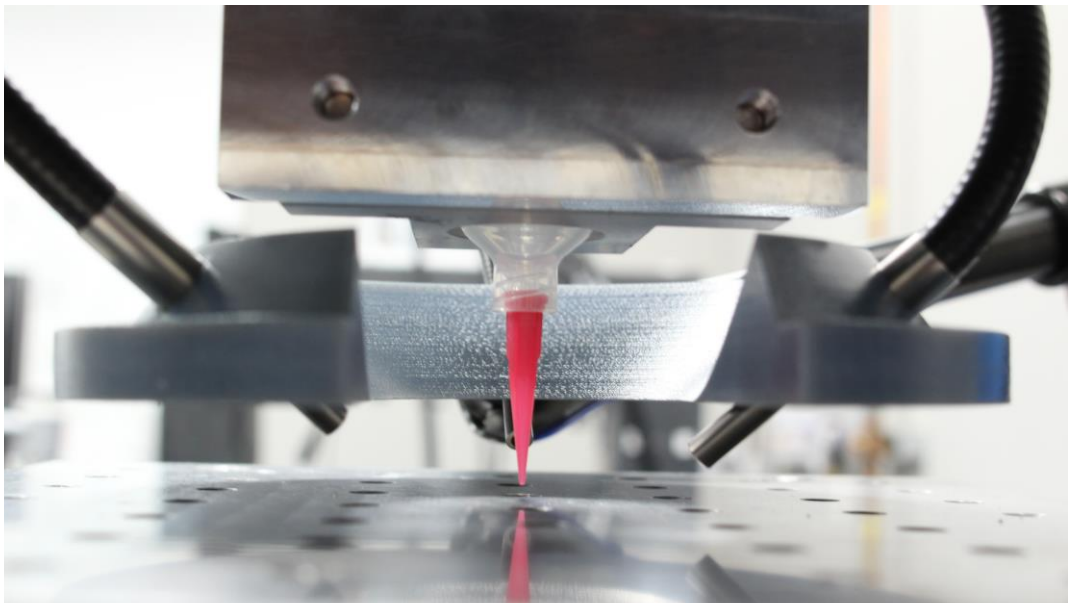

Figure S12. Custom on-demand UV curing mount with three light guides focused to a single spot size under the printing nozzle.

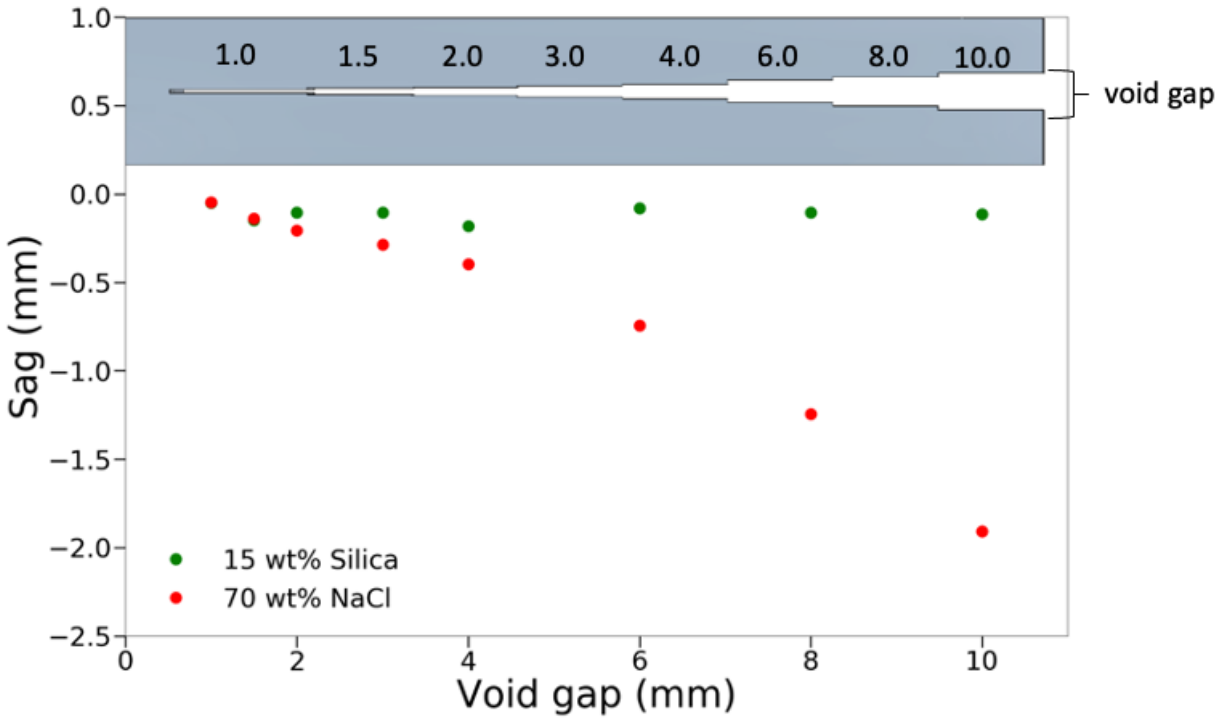

Figure S13: Spanning tests of 70wt% UGAP-NaCl and 15wt% UGAP-FS overlaying a model of a spanning block. Diagram at the top of the graph represents the spanning test block with increasing void gaps in mm.